Journal of Materials Chemistry A

Accepted Manuscript

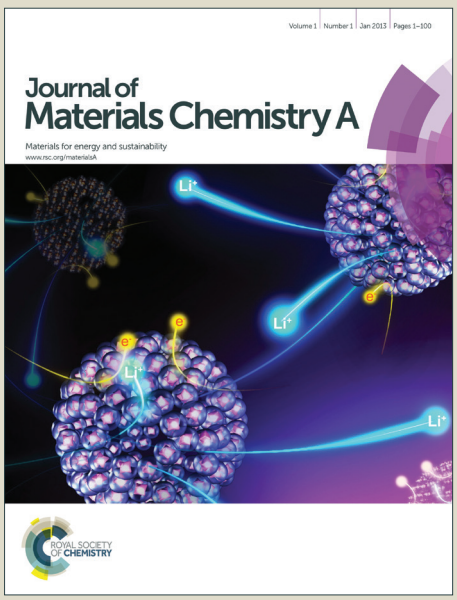

ROYAL SOCIETY OF CHEMISTRY

www.rsc.org/materialsA

Journal Name

RSCPublishing

ARTICLE

Novel AuPd Nanostructures for Hydrogenation of 1, 3-Butadiene

Cite this: DOI: 10.1039/xoxxoooooox

Huimei Chen, [a,b] Jiale Huang,[a,c†] Dengpo Huang, [a] Daohua Sun, [a] Minhua Shao[c†] and Qingbiao Li[a,b,d]

Received ooth January 2012,
Accepted ooth January 2012

DOI: 10.1039/xoxxoooooox

www.rsc.org/

Exotic AuPd bimetallic nanoflowers (NFs) are facilely synthesized using a microorganism-mediated, cetyltrimethylammonium chloride (CTAC)-directed method at room temperature. The NFs consist of one-dimensional long pedicels and three-dimensional open horns. The effect of cell dosage and feed concentrations of ascorbic acid (AA), CTAC and metal precursors on the morphology of bimetallic nanostructures were studied. The results showed that all the obtained materials were alloys with Pd-enriched surfaces. The diameters of horns decreased while those of pedicels increased with increasing the feeding concentration of Pd precursor. The presence of Pd precursor was vital for the formation of the nanowire part of the NF structure. Furthermore, the AuPd-NF/microorganism materials exhibited excellent catalytic performance and durability toward hydrogenation of 1, 3-butadiene.

Introduction

Metals have found extensive use in applications ranging from catalysis to electronics, photonics, information storage, sensing, imaging, medicine, photography, as well as generation, conversion, and storage of energy.[1] With the development of nanotechnology, fabrication of metal nanostructures that maximizes the surface area of metals with tunable shapes and properties has been intensively studied in the past decade.[1, 2] It has been thought that bimetallic nanostructures might outperform the corresponding monometallic nanostructures due to synergetic effect in catalysis.[2] At present, various methods including co-reduction,[2, 3] pyrolysis,[4] seed-mediated method,[5] hydrothermal method,[6] galvanic replacement, etc. [7-9] have been developed to fabricate bimetallic nanostructures with various shapes.[2, 3, 6, 7, 9-14] However, shape control of bimetallic nanostructures based on a versatile strategy still remains challenging.

Microbial biosynthesis of metal nanoparticles has been regarded as a novel and viable alternative to chemical and physical methods for synthesis of metal nanostructures.[15-17] It was thought that metal ions can be adsorbed and reduced by the microbial surface, resulting in very small nanoclusters that gradually grew into metal nanoparticles over the microorganisms.[17, 18] However, the shape of the metal nanostructures could not be effectively controlled by microorganisms alone. Inspired by the wet chemical synthesis of tunable Au nanorods in the presence of Au seeds,[19] we tried the microorganism-bound Au nanoparticles with very small size as seeds for shape control of one dimensional gold nanostructures at room temperature. Functional Au-nanowire/microorganism nanocomposites could be obtained with *Pichia pastoris* cells (PPCs) and *Escherichia coli* cells (ECCs) in the presence of hexadecyltrimethylammonium bromide (CTAB).[20, 21] Interestingly, using cetyltrimethylammonium chloride (CTAC) instead of CTAB, such approach could be expanded to the synthesis of chemically difficult-to-synthesize Au nanohorns (Au NHs).[22, 23] Therefore, the microorganism-mediated, surfactant-directed (MSD) synthesis has been proposed as a new method for shape control of metal nanostructures at room temperature.

It is well known that binary metal ions can be simultaneously adsorbed by microorganisms. The nanoparticles formed by the reduction of microorganism-bound binary metal ions can be nuclei for the growth of novel bimetallic nanostructures. The advantage of the MSD approach is to obtain bimetallic nanostructures in one pot at room temperature. Furthermore, the problem of metal leaching that occurs in galvanic replacement reaction for synthesizing bimetallic nanostructures can be circumvented. In addition, the bimetallic nanostructures can form application-oriented nano-composites with microorganisms. In terms of these premises, we describe a proof of concept of MSD approach to synthesize novel AuPd bimetallic nanoflowers (NFs) consisting of one dimensional pedicel and three dimensional horn in this study. Such NFs have not been reported hitherto, partially due to extreme difficulty in synthesis by pure chemical reduction method. The as-obtained AuPd-NF/microorganism nano-composites can be directly used as an efficient catalyst for hydrogenation of 1, 3-butadiene. This work opens a new avenue to shape control of novel bimetallic nanostructures, which should find promising applications in catalysis.

Experimental Section

Materials and Methods. The same *Pichia pastoris* GS115 cell powder in the previous work was employed in this work. Chloroauric acid ($HAuCl_4$), palladium chloride ($PdCl_2$),

cetyltrimethylammonium chloride (CTAC) and ascorbic acid (AA) were all purchased from Sinopharm Chemical Reagent Co. Ltd. in China. Deionized (DI) water was used throughout this work.

Preparation of AuPd bimetallic nanostructures. Three steps were adopted in a typical synthesis of AuPd bimetallic nanostructures. Firstly, dried PPCs (0.005 or 0.01 g) were added to 10 mL of aqueous CTAC solution (1.0, 5.0, 10.0 or 15.0 mM) in a flask. Next, aqueous $HAuCl_4$ (48.6 mM, 0.0514 mL) and H_2PdCl_4 (0.05 M, 0.050 mL) solutions were added to the mixture. Finally, 0.05, 0.1 or 0.5 mL AA (0.1 M) was added to the mixture. The color of the solution turned from orange red to light orange immediately after adding the AA solution. The flask was then shaken on a shaker (30 ^oC, 150 rpm) for 1-24 h. A few precipitates were observed at the bottom of the flasks after 0.5 h of reaction while the color of the solution turned to black. The final AuPd/PPC samples were centrifuged at 2000 rpm for 10 min and dispersed in 200 uL of deionized water for further characterizations. It should be noted that aqueous Au and Pd solutions were added into the mixture via three different modes. For Mode A, Au and Pd precursors were simultaneously added into the mixture, and then allow 50-min interaction between the cells and metal ions before adding AA concentration; For Mode B, Au precursor was added after Pd precursor reacted for 50 min; Mode C is the reverse of Mode B.

Characterizations of AuPd bimetallic nanostructures. Transmission electron microscopy (TEM) characterization was performed on an electron microscope (Tecnai F30, FEI; Netherlands) with an accelerating voltage of 300 kV. Scanning electron microscopy (SEM) samples of the suspension were fabricated by dropping the suspension onto a clean silicon wafer. SEM observations were carried out on a Hitachi S-4800 SEM system. The sizes of AuPd NFs were measured on the basis of SEM images.[24] After the centrifugation, the precipitates were dried at 50 °C in vacuum and taken for x-ray diffraction (XRD) and x-ray photoelectron spectroscopy (XPS) analysis, which was performed on a Rigaku Ultima IV X-ray Diffractometer (Rigaku, Japan) and a Quantum 2000 spectrometer using the Al-Kα line as the excitation source, respectively. The binding energy was calibrated by C1s as reference energy (C1s = 284.8 eV). Supernatant solutions were decanted after removing the composites by centrifuging at the first time, in order to analyze the Pd(II) and Au(III) concentrations using atomic absorption spectrophotometer (AAS) (Pgeneral, China). The compositions of Au and Pd in the obtained sample dissolved in aqua regia were also analyzed by AAS.

Hydrogenation of 1, 3-butadiene. The catalytic reactions were carried out at 35 °C in a 1-cm-diameter fixed bed flow stainless reactor under atmospheric pressure using a feed concentration of 2.13% 1, 3-butadiene, 4.29% H_2, and 93.58% N_2.[25] The temperature was measured by using a glass tube covered Cr-Al thermocouple located in the center of the catalyst bed. The catalyst (15 mg of AuPd/PPC composites) was diluted with 50 mg of quartz sand before being loaded into the reactor with a space velocity of 9230 mL h^{-1} $g_{cat.}^{-1}$. The reactor effluent was analyzed online every 20 min within 2 h period using a gas chromatograph (GC) equipped with an Al_2O_3 column and a FID detector. The conversion of 1, 3-butadiene and selectivity to butene (*trans*-2-butene, 1-butene, or *cis*-2-butene) or butane were calculated.

Results and Discussion

Synthesis and characterizations of AuPd bimetallic nanoflowers

Effect of metal precursors adding mode. Following our previous work on synthesis of Au NHs,[22, 23] the MSD approach was expanded to bimetallic nanostructures in this work. Interestingly, as shown in Figure 1, exotic NFs comprising one-dimensional pedicels (nanowires) and three-dimensional open nanohorns were obtained by reducing $HAuCl_4$ and H_2PdCl_4 (0.25 mM, Au/Pd ratio of 1:1, Mode A and B) in the presence of AA (1.0 mM), PPCs (5 mg) and CTAC (5.0 mM). The diameters of the pedicels and horns were denoted as d_p and d_h, respectively. To the best of our knowledge, similar nanostructures have not been reported hitherto. On the basis of Mode A and B, approximate d_h of the as-synthesized NFs were obtained, ca. 0.26±0.08 μm (Figure S1 in Supporting Information). However, d_p of the NFs by mode A (31.1±6.9 nm) was much larger than that by Mode B (18.8±4.6 nm) (Figure S1). As revealed by EDX spectra (Figure S2), the local Au/Pd ratio of the NFs was about 1.27. The overall Pd/Au atomic ratio was further determined to be ca. 0.80 by AAS analysis, lower than the initial ratio of 1.0 (Figure S3). The reduction potential of $[AuCl_4]^-$/Au ($[AuCl_4]^-$/Au = + 1.002 V vs. standard hydrogen electrode (SHE)) is higher than that of $[PdCl_4]^{2-}$/Pd ($[PdCl_4]^{2-}$/Pd = + 0.591 V vs. SHE).[26] That is, $AuCl_4^-$ is easier to be reduced than $[PdCl_4]^{2-}$. As a result, ca. 20% Pd was left in the solution, which greatly reduced the Pd leaching compared with galvanic replacement reaction. In contrast to Mode A and B, Mode C led to the formation of nanoparticles (NPs) (74.7±8.8 nm, Figure S4) rather than NFs. To prepare the AuPd bimetallic NFs, further characterizations and synthetic study of the NFs were based on the facile Mode A.

The AuPd NFs on the basis of Mode A were further characterized by TEM, HRTEM, SAED and EDX line profiles. TEM image (Figure 2a) indicates that the open nanohorns connected with thin pedicels to form a NF structure. HRTEM images (Figure 2b and 2c) and the corresponding fast Fourier transform (FFT) pattern (insets in Figure 2b and 2c) show that the corresponding blossom and pedicel are polycrystalline with well-defined lattice planes. The d-spacing of blossom was about 0.230 nm, matching the in-between value of the face-centered cubic (fcc) Au(111) and Pd(111) planes.[12, 27] Another *d* spacing for adjacent lattice fringes of the pedicel was 0.250 nm, which corresponds to the forbidden 1/3{422}.[28] And the common (111) plane could be also determined from the pedicel (Figure S5). The typical SAED pattern (Figure 2d) from the AuPd NFs shows Bragg reflections of {111}, {200}, {220} and {311} of fcc AuPd. EDX elemental line scanning of an individual AuPd nanowire (pedicel) (Figure 2e) illustrates that they were composed of Au and Pd, demonstrating their bimetallic alloy nature. Next, controlled experiments were further performed to study the effect of the CTAC, AA and Pd concentrations, and the cell dosage on the morphology of the AuPd NFs.

Effect of CTAC. Figure 3 shows SEM images of AuPd NFs synthesized by varing the feeding concentration of CTAC (C_{CTAC}), given the same other conditions. Reducing the CTAC concentration from 5.0 (Figure 1) to 1.0 mM (Figure 3a), long nanowires with buds at one end were obtained. The nanostructures did not change with CTAC concentration doubled from 5.0 to 10.0 mM (Figure 3b) while the d_h slightly decreased to 0.25±0.06 μm (Figure S6a) from 0.26±0.08 μm. When the CTAC concentration was further increased to 15.0

mM, the d_h of the NF structures became much larger (0.51±0.2 μm, Figure 3c, Figure S6b). As demonstrated in our previous reports,[22, 23] CTAC had a great impact on the morphology of the nanostructures. The CTA^+ ions released from CTAC could promote the anisotropic growth of nanostructures. When CTAC was replaced with octadecyltrimethylammonium chloride (OTAC) and dodecyltrimethylammonium chloride (DTAC) with a concentration of 5.0 mM, small NPs instead of NF structures were formed (Figure S7). If CTAC was replaced with CTAB, only nanowires were obtained due to the co-existence of CTA^+ and Br^-. Thus, CTAC was favorable to the formation of the AuPd NFs.

Effect of AA. As a mild reducing reagent, AA also had a strong effect on the morphology of AuPd nanostructures. Figure 4a and 4b depicts the SEM images of AuPd nanostructures prepared at the initial AA concentration (C_{AA}) of 0.5 and 5.0 mM, respectively. Interestingly, the uniform smooth nanowires without horn-like structures (Figure 4a) were obtained by halving the AA concentration used in Figure 1. In addition, the d_p of the nanowires (22.3±4.7 nm, Figure S8a) was smaller than that in Figure 1a (31.1±6.9 nm). By increasing the AA concentration to 5 mM, the horn-like structures remained with shorter pedicels. The d_h of the nanohorns in Figure 4b was 0.29±0.14 μm that was slightly larger than that in Figure 1a (Figure S8b). To demonstrate the distribution of Pd and Au in the nanostructures, STEM elemental mapping characterization was carried out. Figure 5a and 5b indicates the homogeneous distribution of Au (green) and Pd (orange) in the NW and NF structures, respectively.

Effect of cell dosage. The Effect of the cell dosage (m_{cell}) on the shape of nanostructures was also examined. Without PPCs, irregular petals and rough nanobelts were obtained (Figure 6a). In contrast, AuPd NFs were produced in the presence of PPCs. Our previous studies showed that the biosorption of Au(III) and Pd(II) ions by the PPCs was rather rapid.[17, 18] That is, Au(III) and Pd(II) ions can be easily bound to the cells. As a result, the binding sites acted as preferential nucleation sites for the growth of AuPd NPs that would further evolve into AuPd NFs under the direction of CTAC. The effect of the PPC dosage on the morphology of the bimetallic nanostructures was further investigated. Compared with Figure 1, if doubling the cell dosage from 5.0 to 10.0 mg, the NFs with shorter and thicker pedicels (Figure 6b) were attained. Thus, more AuPd NPs distributed over the cell surface by increasing the number of cells. However, AuPd NPs were less concentrated over PPCs, which prevented the formation of potential AuPd NFs. Hence, excess amounts of PPCs could form shorter and thicker pedicels rather than AuPd NFs. Therefore, the appropriate amount of PPCs should be determined to form well-defined AuPd NFs. The PPCs have dual functions, i.e., in the biosorption of binary metal ions and as a platform for preferential nucleation.

Effect of Pd concentration. By comparison with our previous work on Au NHs,[22, 23] the AuPd NF with long pedicel nanostructure was produced by introducing Pd into the system. In other words, the nanowire morphology (pedicel) was promoted. Thus, the effect of initial Pd:Au ratio on the morphology of nanostructures was investigated. The Pd:Au ratio of X: 5 (X=1, 3, 5, 7, 9) was adjusted by changing the Pd precursor concentration while keeping the Au precursor concentration constant. Figure 7 shows SEM images of AuPd nanostructures synthesized at different Pd:Au ratios apart from Pd:Au ratio of 5:5 for Figure 1a. When a small amount of Pd (Pd:Au ratio = 1:5) was added, petals with rough multi-serrated-like nanobelts were obtained without pedicels (Figure 7a). Well-defined NFs structures with long thin pedicels were formed with increasing Pd:Au ratio to 3:5(Figure 7b). The morphology in Figure 7b was very similar with that in Figure 1 (Pd:Au ratio=5:5). If further increasing the Pd content, pedicel structures still retained while horn-like structures disappeared. Instead, nanoparticles or two-dimensional broom at the end of wire appeared (Figure 7c-d). It was found that the diameters of horns gradually decreased with increasing the Pd concentrations, i.e., d_h were 0.69±0.27, 0.29±0.09 and 0.24±0.06 μm (Figure S9a-c) corresponding to Figure 7a-c, respectively. Conversely, the diameters of nanowires increased from 27.8±7.3 to 34.8±5.5 nm (Figure S9d-f). Therefore, the formation of nanowires was attributed to Pd in this system. In the previous report, Zhu et al. also demonstrated that Pd played a crucial role in forming the nanowire morphology in the alloy nanostructure.[9]

To investigate the structures, valence states and elemental distributions of the prepared materials at different Pd:Au ratios, XRD, XPS and HAADF-STEM characterizations were carried out. The XRD results (Figure 8a) show that the diffraction peaks of different Pd:Au ratios are located between those of pure Au (pdf2 card: 00-002-1095) and Pd (pdf2 card: 01-087-0635), which can be indexed to the (111), (200) and (220) of the fcc structure of Au and Pd. The (111) diffraction peak exhibits a shift from pure Au to pure Pd with increasing the Pd content (see inset of Figure 8b). And a good linear relationship was found between the diffraction angles and the Pd mole fractions in Figure 8b. According to Vegard's law, this linear relation indicated that the prepared AuPd nanostructures were alloy and the composition of each bimetallic nanostructure was proportional to that of the feeding solution.[11, 12, 29]

XPS was adopted to study valence states and surface compositions of Au and Pd at different Pd:Au ratios. Figure 9a shows the XPS peaks of Au(0) $4f_{7/2}$ and $4f_{5/2}$ for PdAu nanostructures. The binding energies shift gradually to lower energies as the Pd content increases. Interestingly, the binding energies of Pd(0) $3d_{5/2}$ and $3d_{3/2}$ shifts gradually to higher energies with increasing Pd content, as shown in Figure 9b. The binding energies were summarized in Table S1. The slight shifts in binding energy indicated the changes in electronic properties of both Au and Pd on/near the surface of NF materials, further verifying the formation of the alloy nanostructures.[27, 30] According to the XPS results, all AuPd alloy nanostructures have Pd-enriched surfaces (see last column in Table S1). That is, the Pd:Au ratios of surfaces were much higher than the actual ratios derived from AAS measurements. And the actual Pd/Au ratio was lower than the theoretical one for each sample (Figure S3). The formation of the Pd-enriched surface of AuPd alloy nanostructures may be due to the different reduction rates of Au(III) and Pd(II) species. Considering the reduction potential discussed above, it can be assumed that Au nuclei formed first, then followed by adding Au and Pd atoms onto the nuclei.[11] As a result, the alloy nanostructures with Pd-enriched surfaces were formed.

Figure 10 shows STEM and STEM elemental mapping of AuPd alloy nanostructures at five Pd:Au ratios, which provide insight into both morphology and distribution of Au and Pd with increasing Pd concentration. From left to right, shown in Figure

10a-e are images of nanostructures with increasing Pd content. From up to down, each color picture represents elemental mappings of one nanostructure. Evidently, the elements Au (green) and Pd (orange) are uniformly dispersed in the nanostructures. Furthermore, the morphologies were consistent with the SEM results in Figure 1a and Figure 7.

Formation mechanism of AuPd NFs. As discussed above, the AuPd NFs could be synthesized based on Mode A and Mode B instead of Mode C (the PPCs interacted with Au(III) ions for 50 min prior to addition of Pd precursor). The pronounced difference showed that the Pd ions should occupy some binding sites over the cell surface as the Au(III) ions are more easily reduced than Pd(II) ions. If Au precursor was added prior to Pd precursor, the Au(III) ions rapidly adsorbed on the cell surface. As a result, only a limited amount of binding sites on the cell surface was available for Pd(II) ions. The preferential nucleation sites on the cell surface would be predominantly occupied by Au nuclei, posing the difficulty in adding Pd atoms onto the sites. For Mode B, the Pd(II) ions occupied many binding sites while fewer sites were left for Au(III) ions, still leading to the same NF structures. Under these circumstances, tandem reactions played an important role in promoting the NF nanostructures. The first reaction was reduction of Pd(II) ions to Pd(0) by AA. Then the resulting Pd(0) acted as reductants for the reduction of Au(I) (even Au(III)) ions to Au(0) via galvanic replacement. Therefore, we tentatively believe that the tandem reactions were favorable to addition of Au atoms onto the nanostructures even when the nucleation sites were not sufficient for Au(III) ions in the case of Mode B.

Through careful time-resolved TEM studies, the probable growth mechanism of AuPd NFs on the basis of Mode A was studied. When $HAuCl_4$ and $PdCl_2$ were added in the CTAC and PPCs solution, the colour of the solution exhibited orange red at the beginning due to the presence of ligand-substituted anions such as $[AuCl_4]^-$, $[PdCl_4]^{2-}$, CTA^+–Au(III) or $[PdCl_4(CTA)_2]$ complexes.[31-33] Next, Pd(II) and Au(III) ions were both adsorbed on the cell surface. And 50 minutes of adsorption gave rise to a balanced adsorption rate of Pd(II) and Au(III), ca. 66% and 37%, respectively (Figure S10). In the meantime, PPCs and CTAC could act as mild reduction agents,[17, 34] leading to the colour change from orange red to orange due to the reduction of Au(III) to Au(I). The Au(I) anions and Au(I)-CTAC complex were colorless,[22] resulting in a lighter colour of reaction solution. Upon addition of AA, the colour of the solution changed to light orange immediately. As shown in Figure 11a, there are some observable NPs on the cell surface before the addition of AA. It should be noted that CTAC was a very weak reductant at room temperature. Therefore, the NPs were largely resulted from the reduction of metal ions with the cells.[17, 18] The nucleation of AuPd NPs grew quickly and nanowires (pedicels) appeared on the cell surfaces 5 min after the addition of AA. The nanowires preferred to grow at the junction of the two cells (Figure 11b). During this period, the colour of the solution changed from light pink to dark black, indicating that most of Au ions were firstly reduced by PPCs and CTAC while most of Pd ions were reduced by AA. EDX data showed that both NPs and nanowires contained both Au and Pd elements and the percentage Au was higher than that of Pd. The CTA^+ was expected to adsorb onto the crystal nucleus and thus promote the anisotropic growth of nanostructures. After 15 min, three-dimensional horn stretched on the cell surface and the pedicels became longer (Figure 11c) owing to the platforms of the PPCs for large-size nanostructures. Noted that some AuPd NPs tended to adhere to the structures and these NPs would be consumed via Ostwald ripening mechanism later on during the formation of the AuPd NFs. With further growth, larger-size AuPd NFs were formed (Figure 11d). Eventually, in ~1 hour, most of the nanostructures evolved into well-defined AuPd NFs (Figure 1a), through anisotropic growth with the assistance of CTAC and Ostwald ripening of small AuPd NPs.

Based on the TEM images, we proposed the schematic illustrations for the formation of AuPd NFs in Figure 12. Firstly, the interaction of the PPCs with Au(III) and Pd(II) ions for over 50 minutes led to a balanced adsorption of Au and Pd ions onto the PPCs (at Stage I) and some Au(III) were reduced to Au(I). Next, the addition of surplus AA resulted in further reduction of the adsorbed Au(I) and Pd(II) to form AuPd nuclei that acted as preferential nucleation sites for the formation of AuPd NPs on PPCs (at Stage II). Then, under the direction of CTAC, anisotropic growth of AuPd NWs with bud-like structures at the end of wires was preferred (at Stage III). In the end, well-defined AuPd NFs were formed via Ostwald ripening during the aging of the AuPd NFs (at Stage IV).

Catalytic activity of hydrogenation of 1, 3-butadiene. The AuPd-NF/microorganism composites were explored as catalysts for selective hydrogenation of 1, 3-butadiene. The catalytic performances of the AuPd-NF/microorganism catalysts with different Au/Pd ratios were evaluated. The previous Au-NW/PPC composites synthesized by microorganism-mediated,[20] CTAB-directed method were also tested for comparison. Furthermore, Pd-NP/PPC composites by microorganism-mediated, CTAC-directed method (Pd NWs could not be prepared so far) was also evaluated for this reaction. It can be seen from Figure 13a that the Au-NW/PPC composites were inactive for the reaction with very low conversion efficiency. As far as Pd-NP/PPC composites were concerned, they exhibited high selectivity to butene (*trans*-2-butene, 1-butene and *cis*-2-butene). For AuPd-NF/microorganism catalysts, with increasing Pd content, the conversion efficiency increased gradually from 33.2% to 100%, and the selectivity to butene was also improved significantly compared with single Au-NW/PPC and Pd-NP/PPC catalysts. As reported in the literature for the hydrogenation of 1, 3-butadiene,[35, 36] the selectivity to butene could be enhanced by addition of second metal or metal oxide. It was worth pointing out that, for the AuPd-NF/microorganism catalyst (with Au/Pd ratio of 5:3), the selectivity to total butene and single 1-butene could reach 96.5% and 50%, respectively, though the per-pass conversion efficiency was only 65.4%. However, further increasing the Pd:Au ratio to 5:5, 7:5 and 9:5, the conversion efficiency could reach 100% and the selectivity to butene was slightly lower. The difference in the selectivity and conversion efficiency can be attributed to the shift of Pd 3d binding energy of the NFs at different Pd:Au ratios (Figure 9b). Therefore, the catalytic performance was composition-dependent. And the electron density of Pd affected the catalytic performances.[37, 38] By optimizing the reaction conditions, the selectivity and conversion significantly improved, up to 92.6% and 98.4%, respectively (Figure S11). Additionally, the stability of the AuPd NF catalysts was also evaluated and no loss in conversion or selectivity was observed within time-on-stream of 11 h (Figure 13b). Therefore, the AuPd alloy NFs also possesses desired durability in addition to excellent catalytic performance.

Conclusions

In summary, a simple microorganism-mediated, surfactant-directed (MSD) approach was developed to prepare the exotic and closely packed AuPd alloy nanoflowers with composition-dependent catalytic activity for 1, 3-butadiene hydrogenation. The alloy structures were further confirmed by HAADF-STEM, EDX, XRD and XPS techniques. The shape of AuPd alloy nanostructures was influenced by the cell dosages, AA and CTAC concentrations. Particularly, CTAC and AA played critical roles in the morphology control. Moreover, the diameters of pedicels increased while those of nanohorns decreased with increasing Pd content. In addition, Pd element contributed to the formation of nanowire morphology in NF structures and the obtained AuPd/microorganism materials possessed Pd-enriched surfaces. Importantly, the obtained AuPd NFs/microorganism materials exhibited excellent catalytic activity and durability for hydrogenation of 1, 3-butadiene.

Acknowledgements

This work was supported by the NSFC projects (No. 21106117 and 21036004). J. H. is grateful to the Fujian Provincial Administration of Civil Service for the Fujian-Hong Kong joint postdoctoral fellowship. M.S. was supported by a startup fund from the Hong Kong University of Science and Technology.

Notes and references

[a] Department of Chemical and Biochemical Engineering, College of Chemistry and Chemical Engineering, Xiamen University, Xiamen 361005, PR China

[b] Environmental Science Research Center, College of the Environment & Ecology, Xiamen University, Xiamen 361005, PR China

[c] Department of Chemical and Biomolecular Engineering, Hong Kong University of Science and Technology, Clear Water Bay, Hong Kong, PR China

[d] College of Chemistry & Life Science, Quanzhou Normal University, Quanzhou 362000, PR China

† Address correspondence to cola@xmu.edu.cn (J. Huang) and kemshao@ust.hk (M. Shao). Phone: (+86) 592-2183088. Fax: (+86) 592-2184822.

Notes

Electronic Supplementary Information (ESI) available: The corresponding histograms of diameter distribution, SEM images, table of XPS peak positions, product conversion and selectivity in 1, 3-butadiene hydrogenation, adsorption rates of Au and Pd (1:1) adsorbed by the PPCs. See DOI: 10.1039/b000000x/

1 Xia, Y.; Xia, X.; Wang, Y.; Xie, S. *MRS Bull.* 2013, **38**, 335-344.
2 Wu, B. H.; Zheng, N. F. *Nano Today* 2013, **8**, 168-197.
3 Wang, D. S.; Li, Y. D. *Adv. Mater.* 2011, **23**, 1044-1060.
4 Sun, D. H.; Mazumder, V.; Metin, O.; Sun, S. H. *ACS Nano* 2011, **5**, 6458-6464.
5 Ding, Y.; Fan, F. R.; Tian, Z. Q.; Wang, Z. L. *J. Am. Chem. Soc.* 2010, **132**, 12480-12486.
6 Huang, X. Q.; Zhang, H. H.; Guo, C. Y.; Zhou, Z. Y.; Zheng, N. F. Nanocubes. *Angew. Chem. Int. Ed.* 2009, **48**, 4808-4812.
7 Chen, J. Y.; Wiley, B.; Mclellan, J.; Xiong, Y. J.; Li, Z.-Y.; Xia, Y. N. *Nano Lett.* 2005, **5**, 2058-2062.
8 Teng, X.; Wang, Q.; Liu, P.; Han, W.; Frenkel, A. I.; Wen, W.; Marinkovic, N.; Hanson, J. C.; Rodriguez, J. A. *J. Am. Chem. Soc.* 2008, **130**, 1093-1101.
9 Zhu, C. Z.; Guo, S. J.; Dong, S. J. *Adv. Mater.* 2012, **24**, 2326-2331.
10 Ghosh Chaudhuri, R.; Paria, S. *Chem. Rev.* 2012, **112**, 2373-2433.
11 Lee, Y. W.; Kim, N. H.; Lee, K. Y.; Kwon, K.; Kim, M.; Han, S. W.. *J. Phys. Chem. C* 2008, **112**, 6717-6722.
12 Lee, Y. W.; Kim, M.; Kim, Y.; Kang, S. W.; Lee, J.-H.; Han, S. W. *J. Phys. Chem. C* 2010, **114**, 7689-7693.
13 Huang, X. Q.; Li, Y. J.; Chen, Y.; Zhou, H. L.; Duan, X. F.; Huang, Y. *Angew. Chem. Int. Ed.* 2013, **125**, 6179-6183.
14 Hunyadi, S. E.; Murphy, C. J. *J. Mater. Chem.* 2006, **16**, 3929-3935.
15 Tran, D. T.; Jones, I. P.; Preece, J. A.; Johnston, R. L.; Deplanche, K.; Macaskie, L. E. *Nanotechnology* 2012, **23**, 055701.
16 Chen, H. M.; Sun, D. H.; Jing, X. L.; Lu, F. F.; Odoom-Wubah, T.; Zheng, Y. M.; Huang, J. L.; Li, Q. B. *RSC Adv.* 2013, **3**, 15389-15395.
17 Lin, L. Q.; Wu, W. W.; Huang, J. L.; Sun, D. H.; Waithera, N. M.; Zhou, Y.; Wang, H. T.; Li, Q. B. *Chem. Eng. J.* 2013, **225**, 857-864.
18 Chen, H.; Huang, D.; Lin, L.; Odoom-Wubah, T.; Huang, J.; Sun, D.; Li, Q. *J. Colloid Interface Sci.* 2014, **433**, 204–210.
19 Jana, N. R.; Gearheart, L.; Murphy, C. J. *J. Phys. Chem. B* 2001, **105**, 4065-4067.
20 Wang, M.; Kong, T.; Jing, X. L.; Hung, Y. K.; Sun, D. H.; Lin, L. Q.; Zheng, Y. M.; Huang, J. L.; Li, Q. B. *Ind. Eng. Chem. Res.* 2012, **51**, 16651-16659.
21 Yang, H. X.; Du, M. M.; Odoom-Wubah, T.; Wang, J.; Sun, D. H.; Huang, J. L.; Li, Q. B. *J. Chem. Technol. Biotechnol.* 2014, **89**, 1410-1418.
22 Wang, M.; Odoom-Wubah, T.; Chen, H. M.; Jing, X. L.; Kong, T.; Sun, D. H.; Huang, J. L.; Li, Q. B. *Nanoscale* 2013, **5**, 6599–6606.
23 Jing, X. L.; Huang, D. P.; Chen, H. M.; Odoom-Wubah, T.; Sun, D. H.; Huang, J. L.; Li, Q. B. *J. Chem. Technol. Biotechnol.*2014, **89**, DOI: 10.1002/Jctb.4353.
24 Du, M. M.; Zhan, G. W.; Yang, X.; Wang, H. X.; Lin, W. S.; Zhou, Y.; Zhu, J.; Lin, L.; Huang, J. L.; Sun, D. H., et al. *J. Catal.* 2011, **283**, 192-201.
25 Lu, F.; Sun, D.; Huang, J.; Du, M.; Yang, F.; Chen, H.; Hong, Y.; Li, Q. *ACS Sustainable Chem. Eng.* 2014, **2**, 1212-1218.
26 Lee, Y. W.; Kim, M.; Kang, S. W.; Han, S. W. *Angew. Chem. Int. Ed.* 2011, **123**, 3528-3532.
27 Chai, J.; Li, F.; Hu, Y.; Zhang, Q.; Han, D.; Niu, L. *J. Mater. Chem.* 2011, **21**, 17922-17929.
28 Yamamoto, M.; Kashiwagi, Y.; Sakata, T.; Mori, H.; Nakamoto, M. *Chem. Mater.* 2005, **17**, 5391-5393.
29 Sun, D.; Zhang, G.; Jiang, X.; Huang, J.; Jing, X.; Zheng, Y.; He, J.; Li, Q. *J. Matter. Chem. A* 2014, **2**, 1767-1773.
30 Wu, M. L.; Chen, D. H.; Huang, T. C. *Langmuir* 2001, **17**, 3877-3883.
31 Torigoe, K.; Esumi, K. *Langmuir* 1992, **8**, 59-63.
32 Khan, Z.; Singh, T.; Hussain, J. I.; Hashmi, A. A. *Colloids Surf. B* 2013, **104**, 11-17.
33 Zhang, J.; Zhang, L.; Xie, S.; Kuang, Q.; Han, X.; Xie, Z.; Zheng, L. *Chem. Eur. J.* 2011, **17**, 9915-9919.

34 Lee, Y. W.; Kim, M.; Kim, Z. H.; Han, S. W. *J. Am. Chem. Soc.* 2009, **131**, 17036-17037.
35 Goetz, J.; Volpe, M.; Gigola, C.; Touroude, R. *J. Catal.* 2001, **199**, 338-345.
36 Sarkany, A.; Zsoldos, Z.; Stefler, G.; Hightower, J.; Guczi, L. *J. Catal.* 1995, **157**, 179-189.
37 Dantas Ramos, A. L.; Alves, P. D. S.; Aranda, D. A.; Schmal, M. *Appl. Catal. A: Gen.* 2004, **277**, 71-81.
38 Bertolini, J. C.; Delichere, P.; Khanra, B. C.; Massardier, J.; Noupa, C.; Tardy, B. *Catal. Lett.* 1990, **6**, 215-223.

Figures

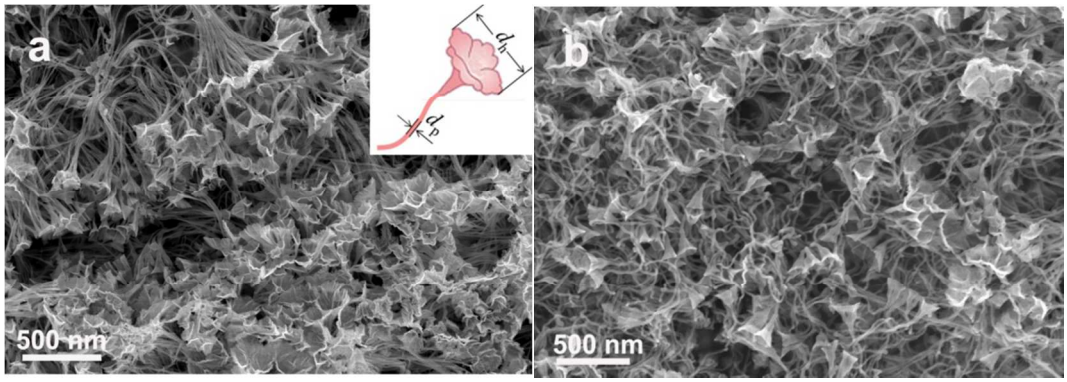

Figure 1. SEM images of AuPd bimetallic nanostructures with a flower structure synthesized through (a) Mode A and (b) Mode B.

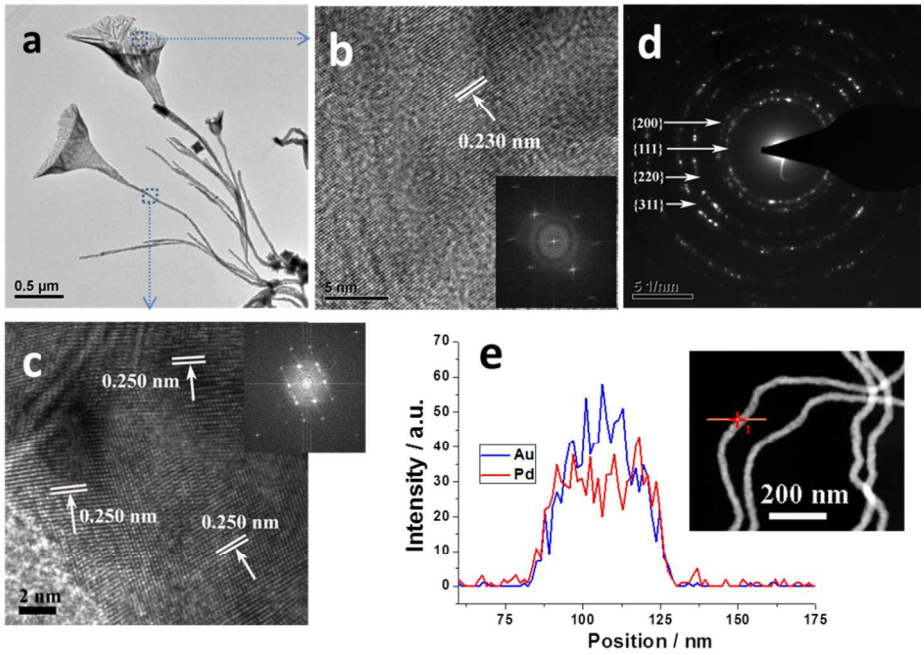

Figure 2. (a) TEM image of AuPd NFs synthesized by Mode A, (b) HRTEM image of blossom, (c) HRTEM image of pedicel, (d) SAED pattern of AuPd NFs, and (e) EDX line profiles of an individual AuPd nanowire (pedicel) corresponding to the framed part (dash) in (a). The insets indicate the corresponding fast Fourier transform (FFT) pattern.

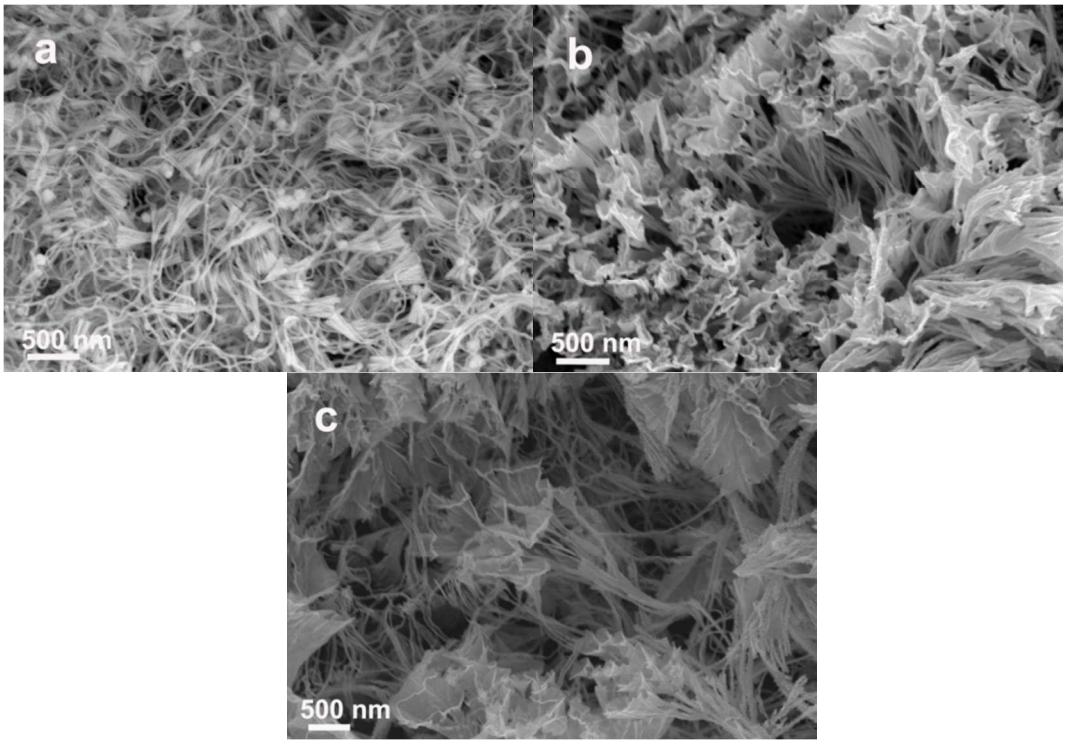

Figure 3. SEM images of AuPd bimetallic nanostructures synthesized by Mode A with various CTAC concentrations of (a) 1.0, (b) 10.0 and (c) 15.0 mM. The initial concentrations of other chemicals were $HAuCl_4$ = 0.25 mM, H_2PdCl_4 = 0.25 mM and AA = 1.0 mM while the dosage of PPCs was 5 mg.

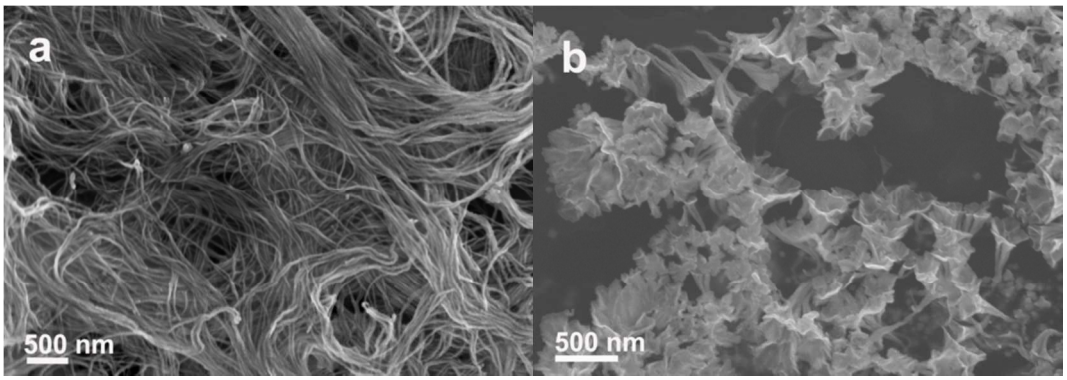

Figure 4. SEM images of AuPd bimetallic nanostructures synthesized by Mode A at the AA concentration of (a) 0.5 mM and (b) 5.0 mM. The initial concentrations of other chemicals were $HAuCl_4$ = 0.25 mM, H_2PdCl_4 = 0.25 mM and CTAC = 5.0 mM while the dosage of PPCs was 5 mg.

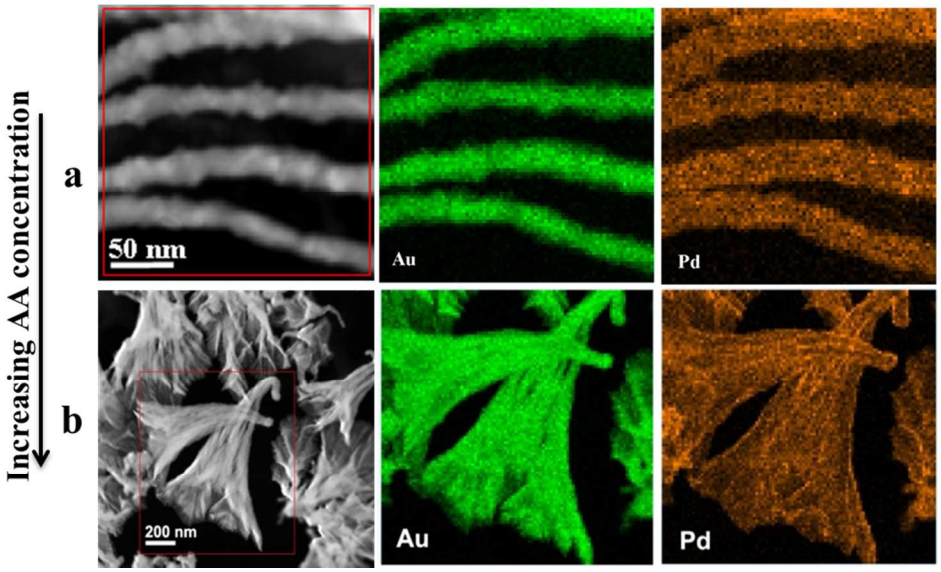

Figure 5. AuPd bimetallic nanostructures characterized by HAADF-STEM and STEM elemental mapping (green indicates Au and orange indicates Pd). The nanostructures were synthesized in the presence of AA with a concentration of (a) 0.5 and (b) 5.0 mM. The initial concentrations of other chemicals were $HAuCl_4$ = 0.25 mM, H_2PdCl_4 = 0.25 mM and CTAC = 5.0 mM while the dosage of PPCs was 5 mg.

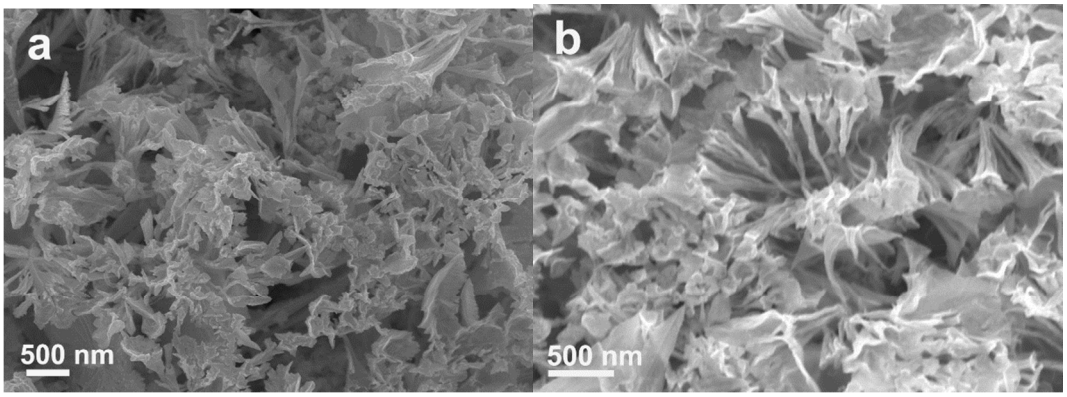

Figure 6. SEM images of AuPd bimetallic nanostructures synthesized through Mode A in the presence of dried PPCs of (a) 0 and (b) 0.01 g. The initial concentrations of other chemicals were $HAuCl_4$ = 0.25 mM, H_2PdCl_4 = 0.25 mM, CTAC = 5.0 mM, AA = 1.0 mM.

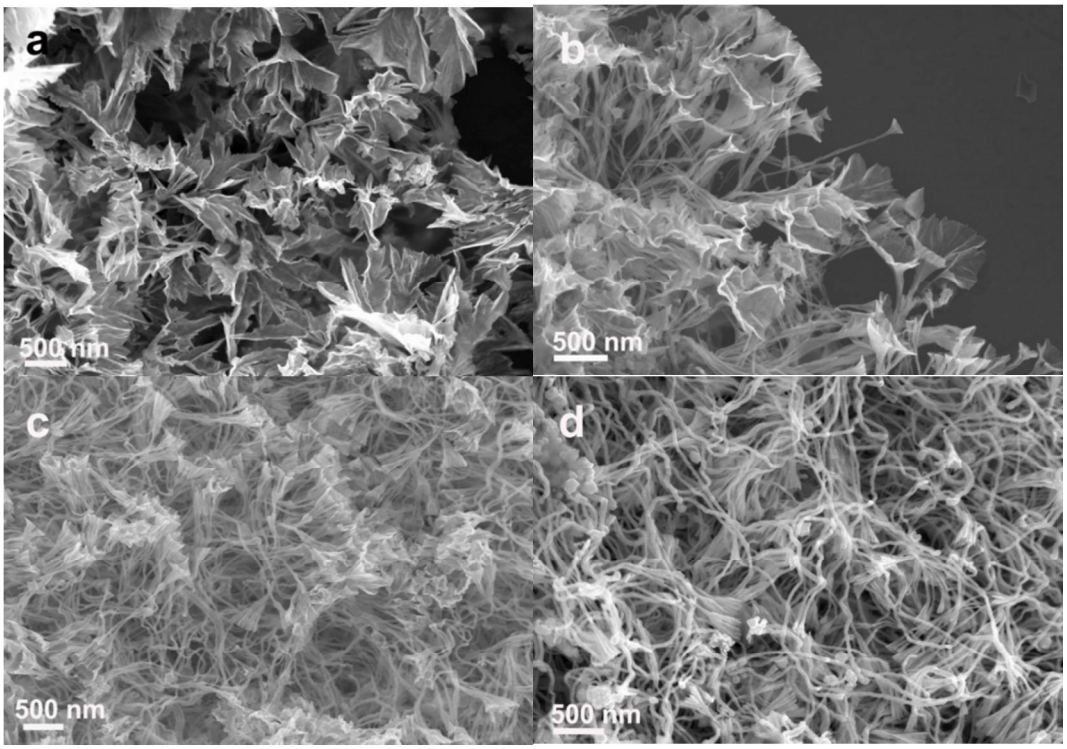

Figure 7. SEM images of AuPd nanostructures synthesized by Mode A at Pd:Au ratios of X: 5 where X is (a) 1, (b) 3, (c) 7, (d) 9. The initial concentrations of other chemicals were $HAuCl_4$ = 0.25 mM, CTAC = 5.0 mM and AA=1.0 mM while the dosage of PPCs was 5 mg.

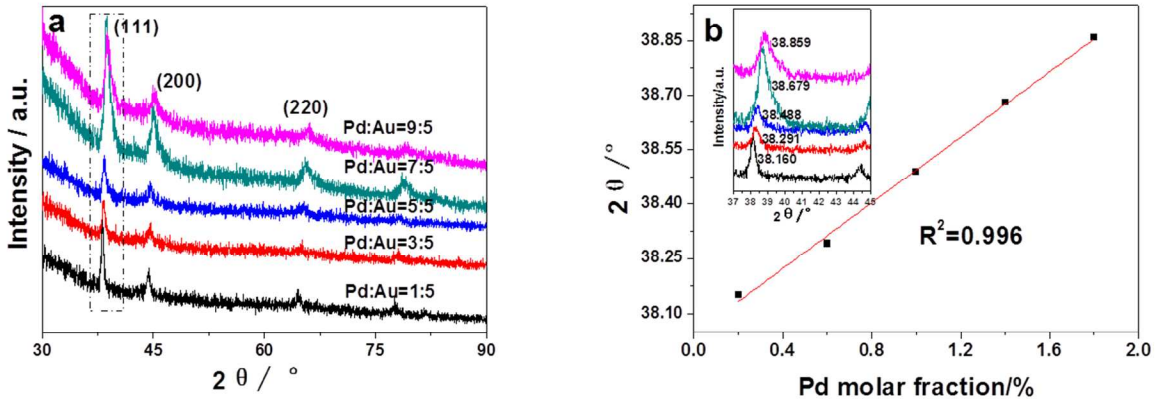

Figure 8. (a) XRD patterns and (b) (111) diffraction peak positions of the AuPd bimetallic nanostructures with different initial AuPd molar ratios.

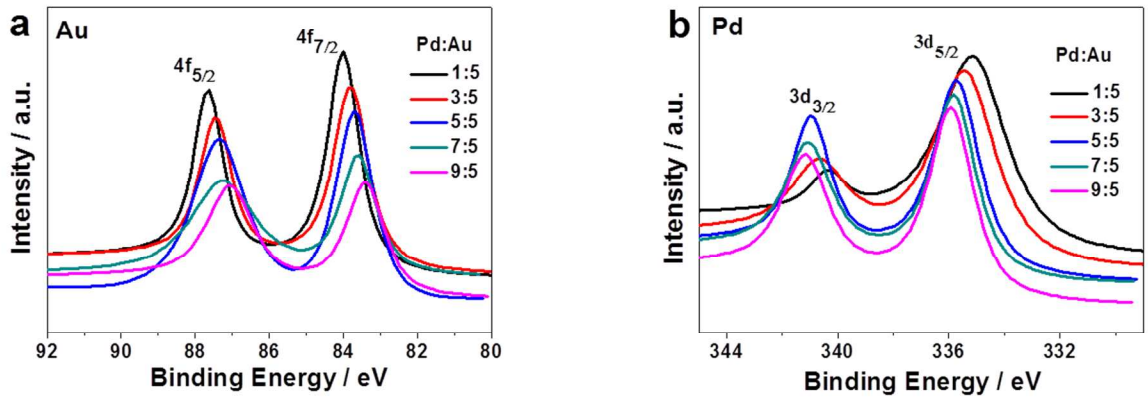

Figure 9. XPS patterns of (a) Au 4f and (b) Pd 3d of AuPd alloy nanostructures with different initial AuPd molar ratios.

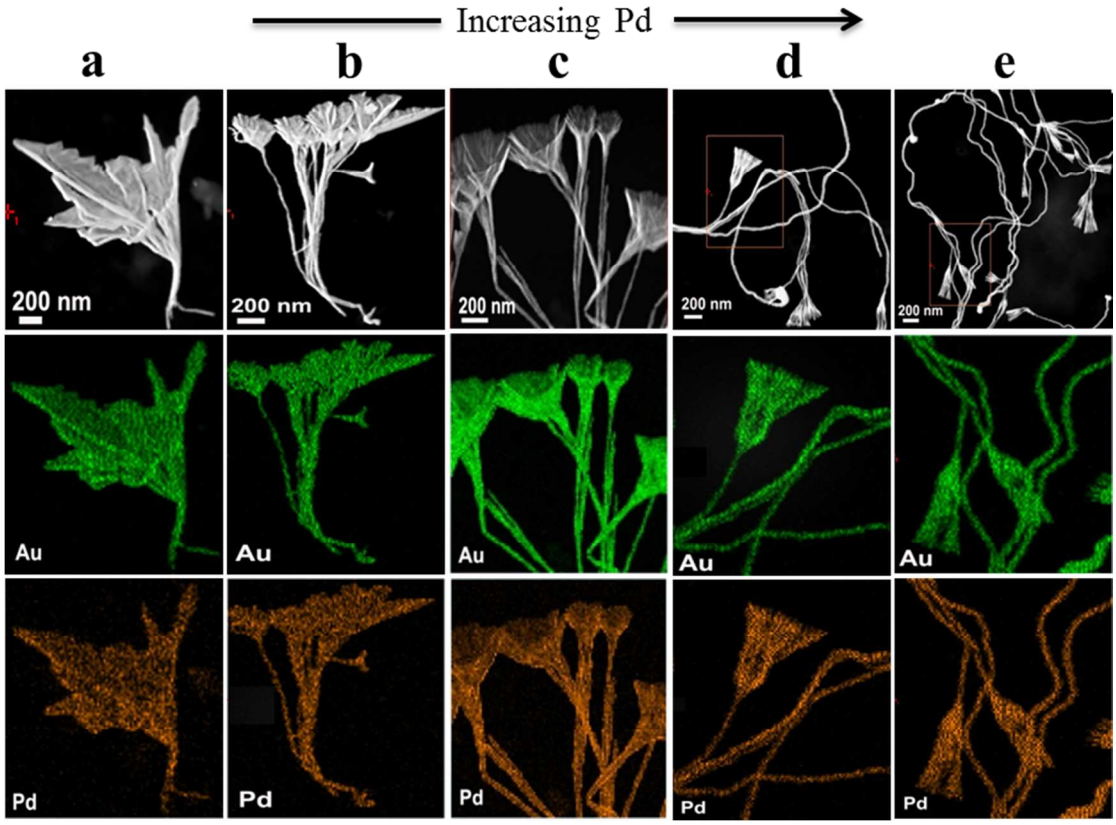

Figure 10. From top to bottom, AuPd bimetallic nanostructures characterized by STEM and STEM elemental mapping (green indicates Au and orange indicates Pd); from left to right, AuPd bimetallic nanostructures synthesized with Pd:Au ratios of X: 5 where X is (a) 1, (b) 3, (c) 5, (d) 7 and (e) 9.

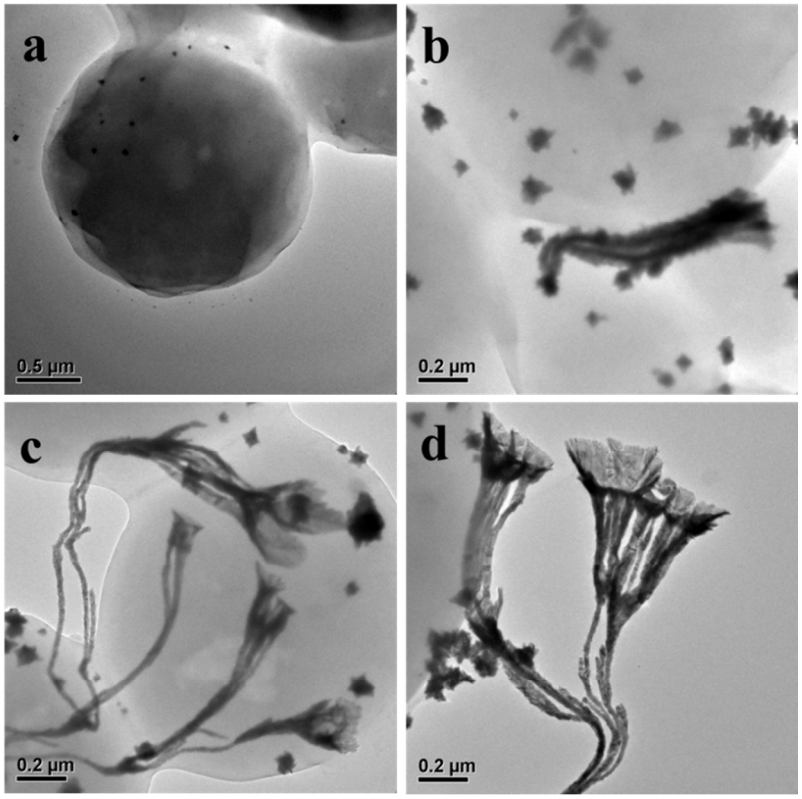

Figure 11. AuPd nanostructures evolution at different time after addition of AA: (a) 0, (b) 5, (c) 15 and (d) 30 min. The synthesis condition is the same with Figure 1a.

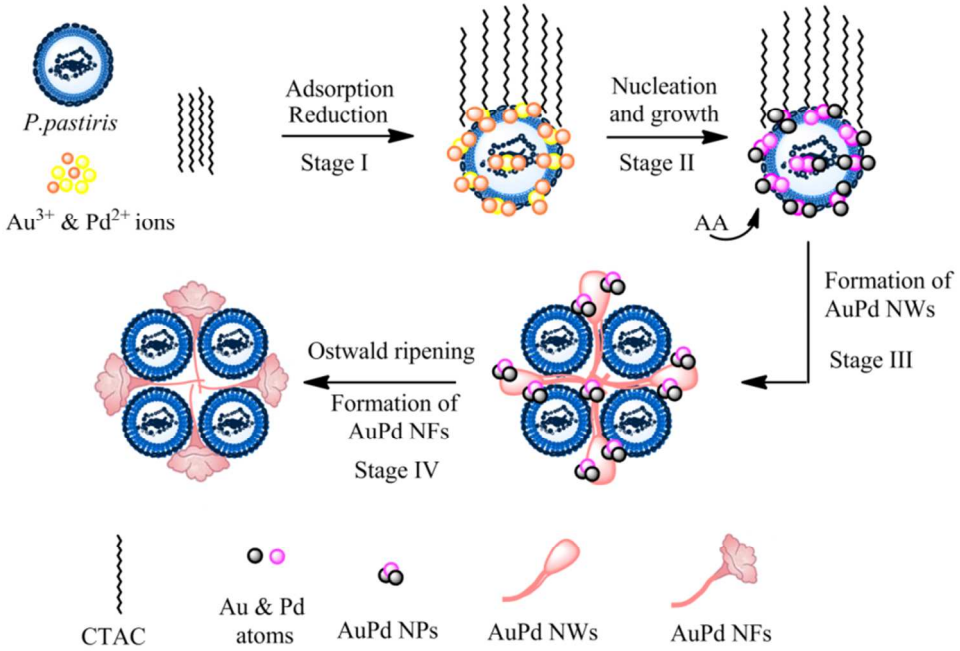

Figure 12. Schematic diagram of the formation of AuPd NFs through the reduction of aqueous $HAuCl_4$ and $PdCl_2$ with AA in the presence of PPCs and CTAC.

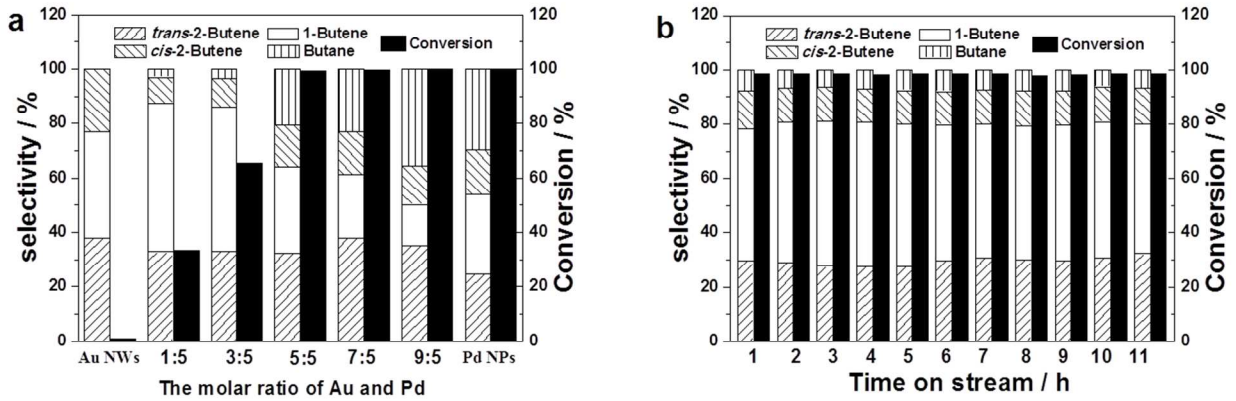

Figure 13. (a) Catalytic performance of the AuPd-NF/microorganism catalysts and (b) the durability of AuPd (1:1) NF/microorganism catalysts in 1, 3-butadiene hydrogenation.

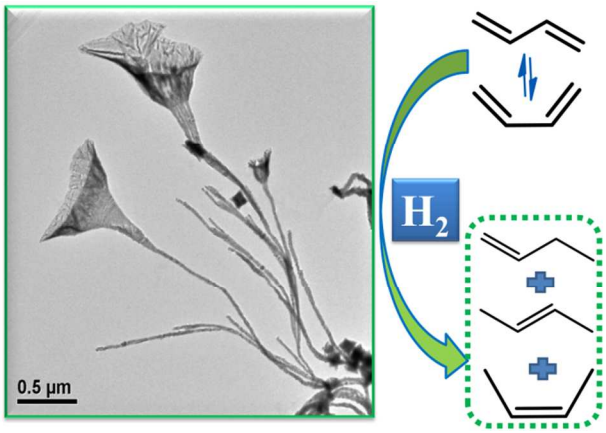

AuPd bimetallic nanoflowers synthesized by a microorganism-mediated method show excellent catalytic performance and durability toward hydrogenation of 1, 3-butadiene.